Investigating the Effect of Different Parameters on Harmonics and EMI Emissions at the Frequency Range of 0–9 kHz

Ganjavi, Amir; Rathnayake, Hansika; Zare, Firuz; Kumar, Dinesh; Abbosh, Amin; Davari, Pooya

Published in:
2020 22nd European Conference on Power Electronics and Applications (EPE'20 ECCE Europe)

DOI (link to publication from Publisher):
10.23919/EPE20ECCEEurope43536.2020.9215815

Publication date:
2020

Document Version
Accepted author manuscript, peer reviewed version

Investigating the Effect of Different Parameters on Harmonics and EMI Emissions at the Frequency Range of 0–9 kHz

Amir Ganjavi[1], Hansika Rathnayake [1], Firuz Zare[1], Dinesh Kumar[2], Amin Abbosh[1], and Pooya Davari[3]

[1] THE UNIVERSITY OF QUEENSLAND
St Lucia,
Brisbane, QLD 4072, Australia
E-Mail: a.ganjavi@uq.net.au, h.rathnayake@uq.edu.au, f.zare@uq.edu.au, and a.abbosh@uq.edu.au

[2] DANFOSS DRIVES A/S
6300 Gråsten, Denmark
E-Mail: dineshr30@ieee.org

[3] AALBORG UNIVERSITY
Aalborg, Denmark
E-Mail: pda@et.aau.dk

Acknowledgements

The authors would like to thank the Australian Research Council, supporting FT150100042 and LP170100902 projects.

Keywords

«Electromagnetic interference (EMI)», «EMI filter», «Frequency dependency», «Harmonics».

Abstract

Due to the increasing use of fast switching semiconductors, emissions affected by the Adjustable Speed Drives (ASDs) are entering the new frequency range of 2–150 kHz. Emissions at this new frequency range are categorised into 2–9 and 9–150 kHz ranges among the standardization communities. Consequently, designing new filters for theses frequency ranges is of the determined efforts by ASD manufacturers. In this paper, essential factors impacting on the filter design in ASDs for 0–2 kHz and the new frequency range of 2–9 kHz are investigated. Non-linear effects of DC link filter on low order harmonic emissions of 0–2 kHz is investigated to understand how the existing filters can comply with the emerging standard of 2–150 kHz. Moreover, a system model is presented to predict the effects of cables and Electromagnetic Interference (EMI) filter parameters on resonances at the frequency range of 2–9 kHz.

Introduction

Adjustable Speed Drives (ASDs) have attracted many applications [1]–[3] owing to the significant advances in power electronics technology. According to the International Electrotechnical Commission (IEC) and International Special Committee on Radio Interference (CISPR), ASD manufacturers should comply with the requirements of the Electromagnetic Compatibility (EMC) for the frequency ranges of 0–2 kHz and 0.15–30 MHz [4]. Therefore, the grid-connected drives should not generate

harmonics/noise exceeding the applicable standard limits. Consequently, implementation of Electromagnetic Interference (EMI) filters at the grid and converter sides of the drive is of great importance.

Due to the high penetration of modern power electronic technologies with fast switching semiconductor devices such as MOSFETs and IGBTs, harmonics are shifting from the low-frequency range of 0–2 kHz to the new frequency range of 2–150 kHz, creating severe power quality problems [4]–[10].

Until now, there is not a precise regulation for the frequency range of 2–150 kHz. Fig. 1 shows the existing harmonic standards developed by various international committees. As seen in Fig. 1, there is a clear gap for the regulation of the 2–150 kHz frequency range [11]. Recently, standardization communities are taking severe steps to define regulations for this new frequency range [12]–[15]. Accordingly, harmonic emissions at the frequency range of 2–150 kHz are known as supra-harmonics among the communities. As a result, motor drive manufacturers are investigating for designing new filters to cover this new frequency range of 2–150 kHz.

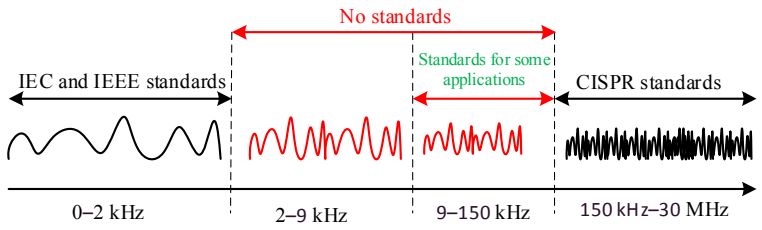

Fig. 1: Harmonic and conducted emission frequency ranges classification.

There are serious challenges to the power electronic engineers to make the existing harmonics/EMI filters compatible with the emerging frequency range of 2–150 kHz. Existing filters that are designed for the 0–2 kHz and 150 kHz–30 MHz frequency ranges may generate resonances for the new frequency range of 2–150 kHz. Besides, the parameters of EMI filter can adversely affect the resonances of the system at 2–150 kHz, which is a critically important factor to design filters for this new frequency range. Also, in practice, characteristics of materials such as permeability, permittivity and skin depth are highly dependent on frequency [16]. As a result, the inductance value of the DC chokes is constant only at a limited range of frequency. This behavior depends on the core permeability, which drops when the frequency is increased, making the existing conventional DC chokes inappropriate to cover the 2–150 kHz frequency range.

Several studies have been carried out in the area of 2–150 kHz frequency range. In [17], harmonic emissions caused by the Active Front End (AFE) inverter at the frequency range of 2–9 kHz are investigated, and the effect of different LCL filters on the emissions is analyzed. Reference [18] investigates the supra-harmonics created by three different photovoltaic inverters through analysing the Fourier series of voltages. Accordingly, it was concluded that several factors such as input DC voltage, fundamental output AC voltage, output voltage waveform, output power and network impedance affect the supra-harmonics caused by the inverters. Furthermore, reference [19] investigates the approaches to improve the EMI performance of the system at the 9–150 kHz frequency range through Differential Mode (DM) filter. In [20], a measurement approach for high-frequency harmonics up to 9 kHz has been presented. In [21], the effect of modulation techniques on supra-harmonics is investigated. Accordingly, Random Pulse-Position Modulation (RPPM) proved highly effective in reducing supra-harmonics. In fact, utilizing RPPM in the two-level inverter almost eliminated the emissions related to the odd multiples of the carrier frequency. Moreover, in [22], the impedance of the grid, which is a crucial factor in power quality issues, has been estimated for the frequency range of 2–150 kHz.

In this paper, essential factors for making the existing low and high-frequency filters compatible with the new frequency range of 2–9 kHz are investigated. Accordingly, the main focus is on coping with the

Common Mode (CM) currents in ASDs to comply with the emerging standards. Due to the considerable impact of frequency dependent passive elements at this range, the ASD system is implemented in a Multiphysics simulation platform, in which components are defined by frequency-dependent materials. This paper is arranged as follows. In the following section, the effect of DC chokes' frequency dependency on low order harmonic emissions of 0–2 kHz is investigated. Then in the next section, a system model is presented in which the CM impedance of the drive system is extracted to predict the effects of cable and EMI filter on the resonances within the 2–9 kHz frequency range. This will be very helpful for the designers to understand the resonances at this frequency range and avoid assigning the switching frequency of the drives at these resonance frequencies. Finally, a conclusion is drawn by the paper.

Effect of nonlinear effects of DC chokes on 0–2 kHz harmonics

Fig. 2 shows the configuration of an ASD analyzed in Multi-physics ANSYS–MATLAB platform. The existing DC-link filters are designed to suppress low order harmonics of 0–2 kHz. Moreover, the EMI filter at the AC side is to suppress the emissions related to the standard of 150 kHz to 30 MHz. As shown in Fig. 2, a Line Impedance Stabilization Network (LISN) is also connected between the grid and EMI filter to isolate the unwanted noises from the power source.

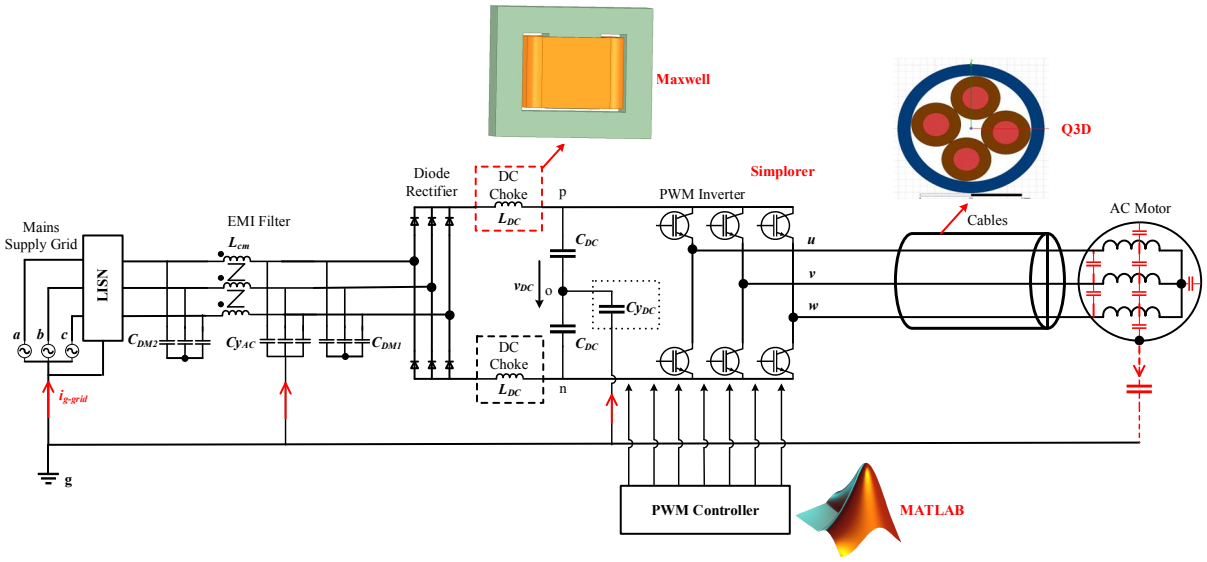

Fig. 2: The implemented ASD system in multi-physics ANSYS–MATLAB platform.

The voltage across the DC link (v_{DC}) contains low order harmonics, which is explained as follows. According to the DC link components of the drive system in Fig. 2, it is assumed that the grid's voltage for phase a of the system (v_a) can be expressed as:

$$v_a(t) = V_m \sin(\omega t) \tag{1}$$

Where V_m is the peak voltage of the grid and $\omega = 2\pi f$. Moreover, according to Fig. 2, the Fourier series of the voltages between different points of the DC link can be calculated as the following equations:

$$v_{pg} = \frac{3\sqrt{3}V_m}{2\pi}\left(1 + \frac{1}{4}\cos(3\omega t) - \frac{2}{35}\cos(6\omega t) - \ldots\right) \tag{2}$$

$$v_{ng} = \frac{-3\sqrt{3}V_m}{2\pi}\left(1 - \frac{1}{4}\cos(3\omega t) - \frac{2}{35}\cos(6\omega t) - \ldots\right) \tag{3}$$

Where v_{pg}, v_{ng} and v_{og} are the voltages across the points p–g, n–g and o–g of the DC link component shown in Fig. 2, respectively. According to Fig. 2 and based on Kirchhoff's Voltage Law (KVL),

$$v_{pn} = v_{po} + v_{on} = \left(v_{pg} - v_{og}\right) + \left(v_{og} - v_{ng}\right) = v_{pg} - v_{ng} \tag{4}$$

Thus, from (2)–(4), the DC link voltage can be extracted as follows:

$$v_{pn} = \frac{3\sqrt{3}V_m}{\pi}\left(1 - \frac{2}{35}\cos(6\omega t) - \ldots\right) \tag{5}$$

According to (5), the DC link voltage (v_{pn}) contains AC terms. This voltage contains a first-order AC term whose frequency is sixth times of the fundamental frequency, and therefore it takes place in the frequency range of 0–2 kHz. Consequently, DC link filters (L_{DC}) are assigned to suppress the low order harmonics created by the diode rectifier. However, these filters face challenges for compatibility with the new range of 2–9 kHz.

In Fig. 3, the frequency behavior of three different types of DC chokes is depicted. Three kinds of frequency-dependent magnetic cores have been simulated in ANSYS Maxwell software to extract inductance of the cores over the frequency range of 0–9 kHz. According to Fig. 3 (a), the ideal DC choke has a constant inductance value in the whole frequency range, but in practice, the inductance value drops with an increase in frequency. Also, in a high-quality DC choke, it is expected that the inductance value smoothly decreases. On the other hand, a low-quality DC choke is also analyzed where the inductance value drops severely to around 50 % of its primary value.

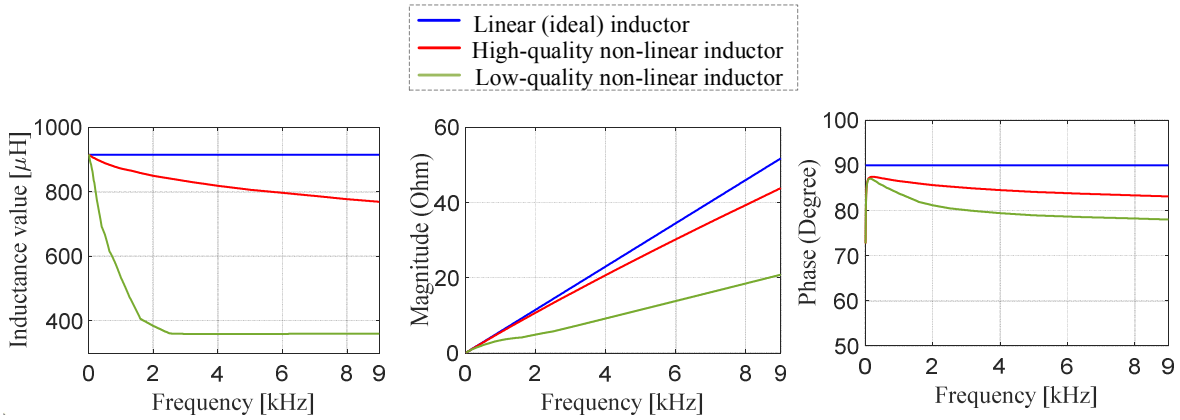

(a) (b) (c)

Fig. 3: Frequency behavior of three types of DC chokes (ideal, high quality and low quality). (a) Inductance, (b) Impedance magnitude, (c) impedance phase.

After assigning the frequency-dependent cores of Fig. 3 in ANSYS Maxwell, these simulated models are linked to the drive system in ANSYS Simplorer to analyze the frequency-dependent model in the time domain simulation. Accordingly, Fig. 4 shows the grid current of the drive system with the aforementioned cores in the time domain. Moreover, the Fast Fourier Transforms (FFTs) of the grid currents are depicted in Fig. 5. According to Fig. 5, when the DC choke is of low quality, the low-frequency harmonics are substantially affected. Also, with the low-quality DC choke, increases of around 0.7 A and 0.4 A in the 5^{th} and 7^{th} order harmonics current magnitudes can be seen, respectively. This finding indicates that nonlinearity of DC choke is an essential factor to design the filters for 0–2 kHz range. Therefore, if the designer aims to make the low-frequency filter compatible with the 0–2 kHz standard, one should provide a high-quality core material, the permeability of which is relatively constant at least up to 9 kHz.

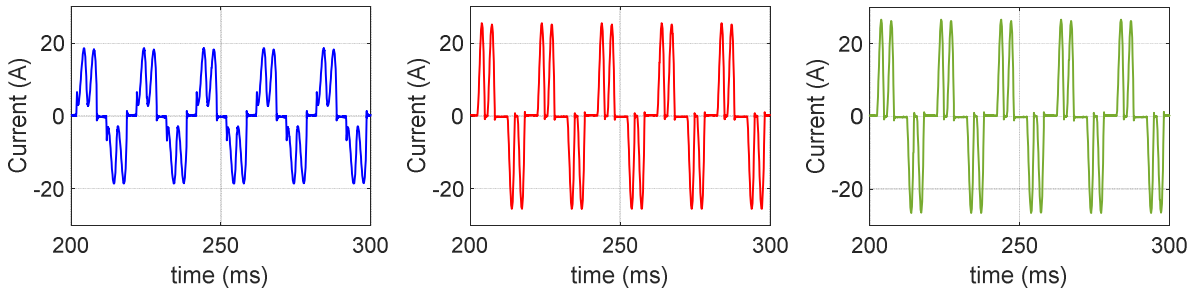

(a) (b) (c)

Fig. 4: Grid current of phase a with different types of DC chokes (the output power is 5.5 kW): (a) Linear ideal chokes, (b) High quality non-linear DC chokes, (c) Low quality non-linear DC chokes.

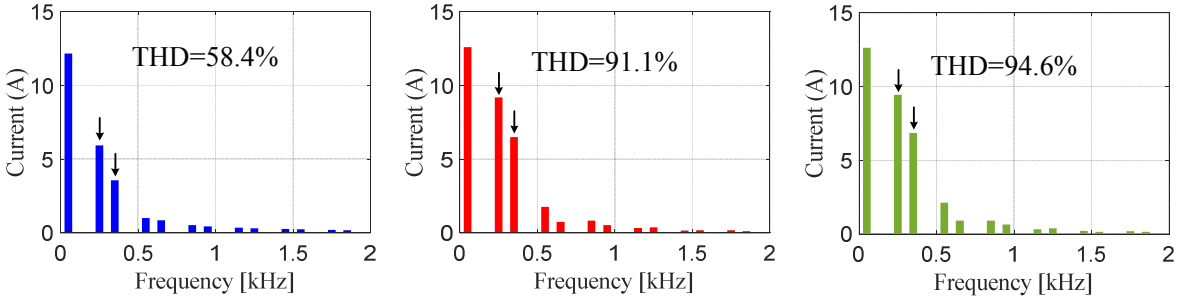

(a) (b) (c)

Fig. 5: FFT of the grid current with different types of DC chokes: (a) Linear ideal chokes, (b) High quality non-linear chokes, (c) Low quality non-linear chokes.

Effects of cables and EMI filter parameters on 2–9 kHz harmonic

According to Fig. 2, phase voltages of the inverter outputs (u, v and w) with respect to DC link midpoint (o) are defined as v_{io} where $i = u$, v, and w. These voltages can be calculated through (6):

$$v_{io}(t) = V_{DC} M \cos(\omega_o t + \theta_i) + \frac{4V_{DC}}{\pi} \sum_{m=1}^{\infty} \sum_{n=-\infty}^{\infty} [\frac{1}{m} J_n(m\frac{\pi}{2}M) \times \sin([m+n]\frac{\pi}{2}) \times \cos(m\omega_c t + n[\omega_o t + \theta_i])] \quad (6)$$

Where M = modulation index, m, n = carrier, baseband index variable, ω_c, ω_o = angular frequency of carrier waveform, fundamental voltage, $J_n(x)$ = Bessel function of order n and argument $x = m\frac{\pi}{2}M$, $\theta_{i=a,b,c} = 0, -\frac{2\pi}{3}, \frac{2\pi}{3}$

Also, the CM voltage (v_{CM}) generated by PWM at the inverter terminal can be derived as (7):

$$v_{CM}(t) = \frac{v_{ao} + v_{bo} + v_{co}}{3} \quad (7)$$

Finally, from (6) and (7), the harmonious AC terms of the CM voltage (v_{CMh}) can be by extracted through (8):

$$v_{CMh}(t)=\frac{4V_{dc}}{3\pi}\sum_{m=1}^{\infty}\sum_{\substack{n=-\infty\\ n\neq 0}}^{\infty}[\frac{1}{m}J_n(m\frac{\pi}{2}M)\times\sin([m+n]\frac{\pi}{2})\times(1+2\cos n\frac{2\pi}{3})\times\cos(m\omega_c t+n\omega_o t)] \quad (8)$$

According to (8), the CM voltage contains harmonics around the multiplicands of the switching frequency ($m\omega_c+n\omega_o$). As a result, due to the advances in fast switching semiconductor devices, modern drive systems are exposed to the CM voltage with harmonics in the frequency range of 2–150 kHz. In this section, the effect of EMI filter parameters on CM model loops of the system is investigated. Moreover, to understand the effect of cables on the CM impedance, first, the cable model is excluded from the system and then it is included.

Without considering the cable between inverter and AC motor

Fig. 6 shows the equivalent circuit of the CM paths for the three-phase drive system modelled through paralleling the CM current routes. In this model, each component of the system namely EMI filter, DC link filter, DC link capacitors and AC motor are modelled by considering the parasitic couplings between elements. Accordingly, the resonances in the system due to the CM current can be predicted through the presented model. According to Fig. 6, there are two noise sources in the system, which can affect the harmonics at the 2–9 kHz range. These noise sources can be modelled by voltage sources, which $V_{CM\text{-}HF}$ and $V_{CM\text{-}LF}$ are created due to the Pulse Width Modulation (PWM) of the inverter and operation of the grid-side rectifier, respectively. For the resonance analysis, the corresponding CM impedances at these voltage sources are extracted as $Z_{T\text{-}HF}$ and $Z_{T\text{-}LF}$, respectively. The LISN network in Fig. 6 is modeled based on IEC TC77A, WG1 committee to standardize the impedance characteristics at the grid point in the 2–9 kHz frequency range [8]. It is to be noted that the high-frequency model of the AC motor is developed based on the experimental measurements using the Bode 100 Vector Network Analyzer. Table I depicts the specifications of the extracted parameters for the presented model in Fig. 6.

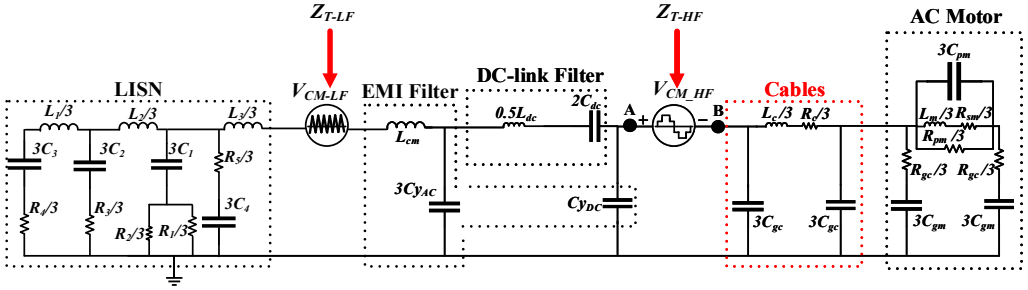

Fig. 6: Equivalent single-phase CM impedance of the system by considering cable parasitic effect.

Table I: Specifications of the drive system

Parameters	Value
L_{dc}, C_{dc}	0.92 mH, 1000 µF
L_m, C_{pm}, C_{gm}, R_{sm}, R_{pm}	9.4 mH,4.5 pF, 1100 pF, 9.5 Ω, 12.7 kΩ
L_c, R_c, C_{gc}	300 µH, 222 mΩ, 20.2 nF
Switching frequency	5 kHz

To survey the effect of cables on the resonances, first, the cables model depicted in Fig. 6 is neglected. Afterwards, to investigate the effect of EMI filter on the system resonances, the parameters of the EMI filter are changed and then $Z_{T\text{-}HF}$ and $Z_{T\text{-}LF}$ are measured using the model presented in Fig. 6. In Fig. 7, the measured parameters of $Z_{T\text{-}HF}$ and $Z_{T\text{-}LF}$ with the aforementioned changes are shown. According to

Fig. 7, with the decrease in the inductance value of the CM choke (L_{cm}) to about 60% of its normal value, the resonant frequency shifts from 1.8 kHz to around 2.2 kHz. Moreover, with a decrease in the capacitance value of the CM filter's capacitance (C_{yAC}) to about 40% of its nominal value, the resonant frequency increases to around 2.8 kHz. Also, it can be seen that with the drop in the capacitance value of C_{yAC}, the magnitude of $Z_{T\text{-}HF}$ at the resonance frequency is substantially decreased, making the system more susceptible to the CM current at this frequency. On the other hand, the magnitude of $Z_{T\text{-}LF}$ is almost unaffected over the wide frequency range even though the resonance is increased with the lower values of C_{yAC} and L_{cm}. In all these cases, the overall magnitude of $Z_{T\text{-}HF}$ is much higher than of the $Z_{T\text{-}LF}$, indicating that $Z_{T\text{-}LF}$ is more critical in the CM current analysis at 2–9 kHz range.

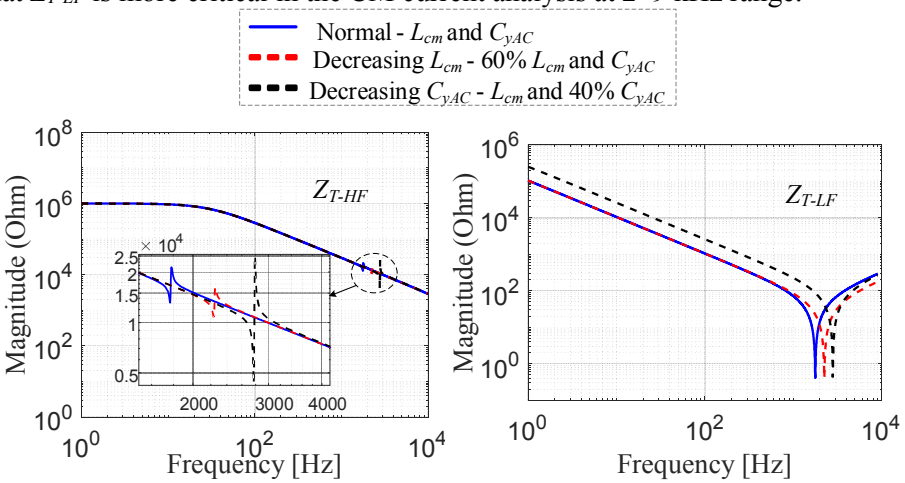

Fig. 7: Modelled CM impedance of the system with different EMI filter parameters (normal case, decreasing L_{cm} to 60% of L_{cm}, and decreasing C_{yAC} to 40% of C_{yAC}); without considering the cable (a) $Z_{T\text{-}HF}$ (b) $Z_{T\text{-}LF}$.

In order to validate the functionality of the extracted CM impedance, time-domain simulations of the studied three-phase motor drive system in Fig. 2 is carried out by MATLAB Simulink. Subsequently, Fig. 8 shows the time-domain waveforms of the grid current $i_{g\text{-}grid}$ (see Fig. 2). Moreover, Fig. 9 shows the harmonic spectrums of i_{g_grid}, which is generated due to the operation of the PWM inverter and rectifier. By comparing Figs. 7 and 9, it can be noted that the extracted $Z_{T\text{-}HF}$ and $Z_{T\text{-}LF}$ can accurately predict the resonance frequencies of the system with different parameters. According to Figs. 9, the harmonic at 5 kHz, which is created due to the switching frequency, has also been increased with a decrease in the values of L_{cm} and C_{yAC}. This is completely aligned with the results related to the modelled system in Fig. 7, in which with a decrease in the values of L_{cm} and C_{yAC}, the CM impedances around the resonance frequencies of the model decreased. These findings are essential steps to predict the level of CM current and the effect of system parameters on the CM current. Consequently, different constraints in the ASD systems such as switching frequency, filter parameters, and cable effects should be considered for the proper filter design.

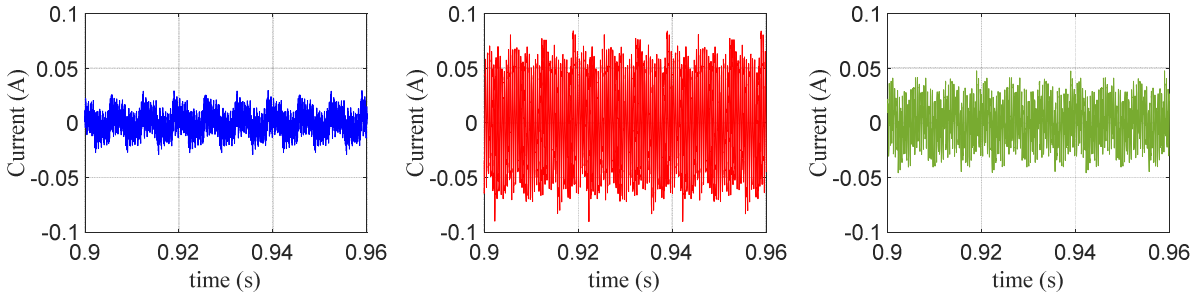

Fig. 8: Time domain ground current $i_{g\text{-}grid}$ for the real system platform; without considering cables. (a) Normal case, (b) decreasing L_{cm} to 60% of L_{cm}, (c) decreasing C_{yAC} to 40% of C_{yAC}.

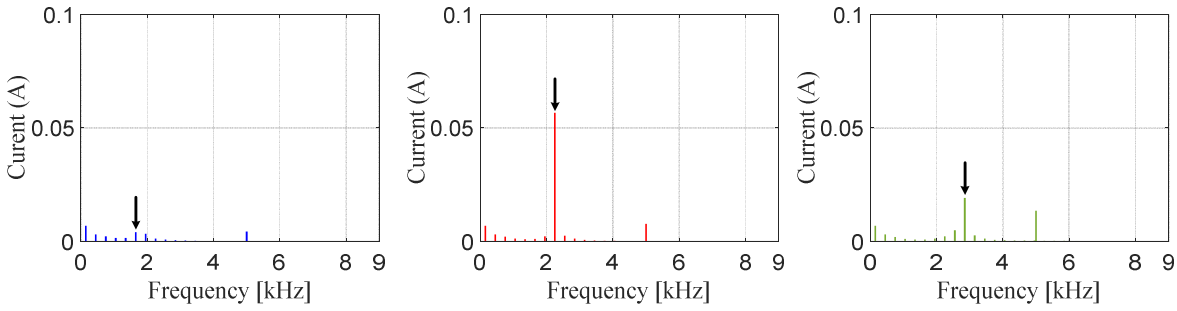

Fig. 9: FFT of the ground current $i_{g\text{-}grid}$ for the real system platform; without considering cables. (a) Normal case, (b) decreasing L_{cm} to 60% of L_{cm}, (c) decreasing C_{yAC} to 40% of C_{yAC}.

Considering the cable between inverter and AC motor

To investigate the effect of cables, now the equivalent model of a general cable seen in Fig. 6 is considered in the system model. The parameters of the cable's high-frequency model can be seen in Table I. Furthermore, Fig. 10 shows the effect of cables on the modelled CM impedances of the system. According to Fig. 10 (a), cables can significantly reduce the magnitude of $Z_{T\text{-}HF}$, making the system more susceptible to resonances. In contrast, cables have no effects on $Z_{T\text{-}LF}$ as can be seen in Fig. 10 (b). Moreover, in Fig. 11, a comparison between the FFT of $i_{g\text{-}grid}$ with and without the implementation of cables is depicted. According to Figs. 10 and 11, *the* behavior of $i_{g\text{-}grid}$ with respect to cables is aligned with $Z_{T\text{-}LF}$ where the effect of cables on $i_{g\text{-}grid}$ is negligible. Moreover, Fig. 12 shows the extracted modelled CM impedances of $Z_{T\text{-}HF}$ and $Z_{T\text{-}LF}$ with different parameters of the EMI filter by considering cables in the system. By comparing Figs. 7 and 12, it can be noted that cables substantially decrease the magnitude of $Z_{T\text{-}HF}$ and subsequently increasing the CM current in the system.

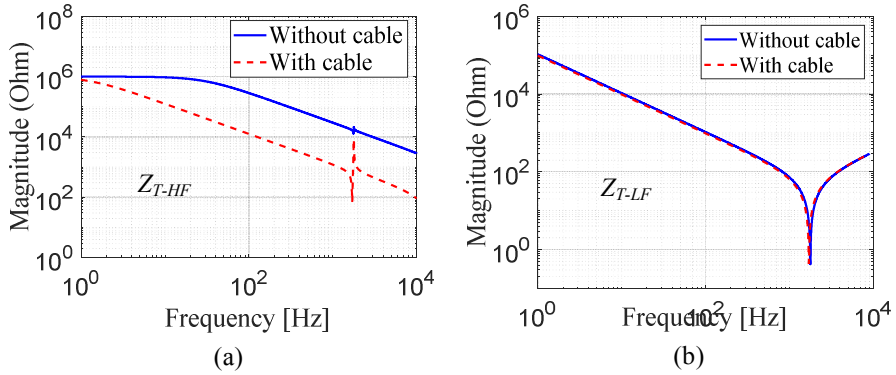

Fig. 10: Cable effects on the modelled CM impedance (a) $Z_{T\text{-}HF}$ (b) $Z_{T\text{-}LF}$.

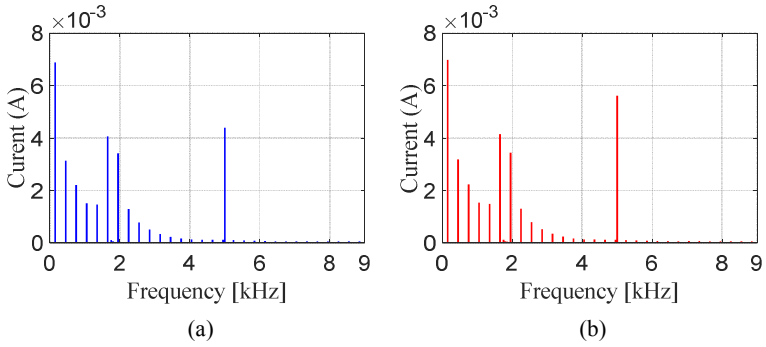

Fig. 11: FFT of $i_{g\text{-}grid}$ in the real system platform. (a) Without cable, (b) with cable.

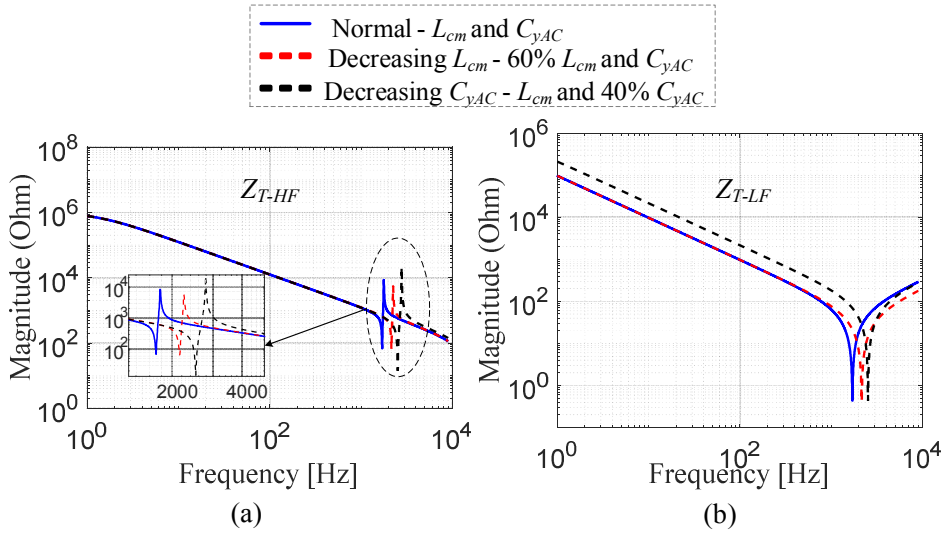

Fig. 12: Modelled CM impedance of the system with different EMI filter parameters (normal case, decreasing L_{cm} to 60% of L_{cm}, decreasing C_{yAC} to 40% of C_{yAC}); with considering cables (a) $Z_{T\text{-}HF}$ (b) $Z_{T\text{-}LF}$.

Conclusion

In this paper, essential factors to design filters for the frequency ranges of 0–2 kHz and 2–9 kHz have been investigated. It is demonstrated that for the frequency range of 0–2 kHz standard, the quality of DC choke can substantially affect the low order harmonics. In fact, with a low-quality inductor whose inductance value harshly decreases with frequency, not only the 5th and 7th order harmonics of the grid currents are increased, but also the emissions above 2 kHz can be affected. To analyze the parasitic behavior of the system at 2–9 kHz frequency range, equivalent CM impedance of the system is modelled. The results verify that the presented model can accurately predict the frequency and magnitude of resonances in the system. The presented model reveals that the EMI filter's parameters can affect the resonance frequencies in the CM loop. Moreover, it is demonstrated that cables significantly reduce the CM impedance at the PWM inverter side, making the system more susceptible to resonances. These findings are significantly important to design filters at the frequency ranges of 0–2 and 2–9 kHz because the designer can have a perception of resonance frequencies to determine parameters of the system such as switching frequency.

References

[1] T. Lubin and A. Rezzoug, "Steady-State and Transient Performance of Axial-Field Eddy-Current Coupling," *IEEE Transactions on Industrial Electronics,* vol. 62, no. 4, pp. 2287-2296, 2015, doi: 10.1109/TIE.2014.2351785.

[2] J. Liu, T. A. Nondahl, P. B. Schmidt, S. Royak, and T. M. Rowan, "Generalized Stability Control for Open-Loop Operation of Motor Drives," *IEEE Transactions on Industry Applications,* vol. 53, no. 3, pp. 2517-2525, 2017, doi: 10.1109/TIA.2017.2661249.

[3] Y. Li, H. Lin, H. Huang, C. Chen, and H. Yang, "Analysis and Performance Evaluation of an Efficient Power-Fed Permanent Magnet Adjustable Speed Drive," *IEEE Transactions on Industrial Electronics,* vol. 66, no. 1, pp. 784-794, 2019, doi: 10.1109/TIE.2018.2832018.

[4] F. Zare, H. Soltani, D. Kumar, P. Davari, H. A. M. Delpino, and F. Blaabjerg, "Harmonic Emissions of Three-Phase Diode Rectifiers in Distribution Networks," *IEEE Access,* vol. 5, pp. 2819-2833, 2017, doi: 10.1109/ACCESS.2017.2669578.

[5] M. H. J. Bollen, P. F. Ribeiro, E. O. A. Larsson, and C. M. Lundmark, "Limits for Voltage Distortion in the Frequency Range 2 to 9 kHz," *IEEE Transactions on Power Delivery,* vol. 23, no. 3, pp. 1481-1487, 2008, doi: 10.1109/TPWRD.2008.919180.

[6] J. Barros, R. I. Diego, and M. d. Apraíz, "A Discussion of New Requirements for Measurement of Harmonic Distortion in Modern Power Supply Systems," *IEEE Transactions on Instrumentation and Measurement,* vol. 62, no. 8, pp. 2129-2139, 2013, doi: 10.1109/TIM.2013.2267451.

[7] J. Yaghoobi, A. Abdullah, D. Kumar, F. Zare, and H. Soltani, "Power Quality Issues of Distorted and Weak Distribution Networks in Mining Industry: A Review," *IEEE Access,* vol. 7, pp. 162500-162518, 2019, doi: 10.1109/ACCESS.2019.2950911.

[8] J. Yaghoobi, F. Zare, T. Rehman, and H. Rathnayake, "Analysis of High Frequency Harmonics in Distribution Networks: 9 – 150 kHz," in *2019 IEEE International Conference on Industrial Technology (ICIT)*, 13-15 Feb. 2019 2019, pp. 1229-1234, doi: 10.1109/ICIT.2019.8755071.

[9] B. John, A. Ghosh, and F. Zare, "Investigation on filter requirements and stability effects of SiC MOSFET-based high-frequency grid-connected converters," *The Journal of Engineering,* vol. 2019, no. 17, pp. 4331-4335, 2019, doi: 10.1049/joe.2018.8033.

[10] P. Kotsampopoulos *et al.*, "EMC Issues in the Interaction Between Smart Meters and Power-Electronic Interfaces," *IEEE Transactions on Power Delivery,* vol. 32, no. 2, pp. 822-831, 2017, doi: 10.1109/TPWRD.2016.2561238.

[11] J. Yaghoobi, A. Alduraibi, D. Martin, F. Zare, D. Eghbal, and R. Memisevic, "Impact of high-frequency harmonics (0–9 kHz) generated by grid-connected inverters on distribution transformers," *International Journal of Electrical Power & Energy Systems,* vol. 122, p. 106177, 2020/11/01/ 2020, doi: https://doi.org/10.1016/j.ijepes.2020.106177.

[12] K. G. Khajeh, D. Solatialkaran, F. Zare, and N. Mithulananthan, "Harmonic Analysis of Multi-Parallel Grid- Connected Inverters in Distribution Networks: Emission and Immunity Issues in the Frequency Range of 0-150 kHz," *IEEE Access,* vol. 8, pp. 56379-56402, 2020, doi: 10.1109/ACCESS.2020.2982190.

[13] S. Sakar, S. Rönnberg, and M. Bollen, "Interferences in AC–DC LED Drivers Exposed to Voltage Disturbances in the Frequency Range 2–150 kHz," *IEEE Transactions on Power Electronics,* vol. 34, no. 11, pp. 11171-11181, 2019, doi: 10.1109/TPEL.2019.2899176.

[14] M. Bollen, M. Olofsson, A. Larsson, S. Rönnberg, and M. Lundmark, "Standards for supraharmonics (2 to 150 kHz)," *IEEE Electromagnetic Compatibility Magazine,* vol. 3, no. 1, pp. 114-119, 2014, doi: 10.1109/MEMC.2014.6798813.

[15] K. G. Khajeh, D. Solatialkaran, F. Zare, and N. Mithulananthan, "Harmonic analysis of grid-connected inverters considering external distortions: addressing harmonic emissions up to 9 kHz," *IET Power Electronics*. [Online]. Available: https://digital-library.theiet.org/content/journals/10.1049/iet-pel.2019.1363

[16] Q. Deng *et al.*, "Frequency-Dependent Resistance of Litz-Wire Square Solenoid Coils and Quality Factor Optimization for Wireless Power Transfer," *IEEE Transactions on Industrial Electronics,* vol. 63, no. 5, pp. 2825-2837, 2016, doi: 10.1109/TIE.2016.2518126.

[17] H. Rathnayake, D. Solatialkaran, F. Zare, and R. Sharma, "Grid-tied Inverters in Renewable Energy Systems: Harmonic Emission in 2 to 9 kHz Frequency Range," in *2019 21st European Conference on Power Electronics and Applications (EPE '19 ECCE Europe)*, 3-5 Sept. 2019 2019, pp. P.1-P.10, doi: 10.23919/EPE.2019.8914845.

[18] M. Klatt, J. Meyer, P. Schegner, and C. Lakenbrink, "Characterization of supraharmonic emission caused by small photovoltaic inverters," in *Mediterranean Conference on Power Generation, Transmission, Distribution and Energy Conversion (MedPower 2016)*, 6-9 Nov. 2016 2016, pp. 1-6, doi: 10.1049/cp.2016.1067.

[19] P. Davari, F. Blaabjerg, E. Hoene, and F. Zare, "Improving 9-150 kHz EMI Performance of Single-Phase PFC Rectifier," in *CIPS 2018; 10th International Conference on Integrated Power Electronics Systems*, 20-22 March 2018 2018, pp. 1-6.

[20] T. Rehman, J. Yaghoobi, and F. Zare, "Harmonic Issues in Future Grids with Grid Connected Solar Inverters: 0–9 kHz," in *2018 Australasian Universities Power Engineering Conference (AUPEC)*, 27-30 Nov. 2018 2018, pp. 1-6, doi: 10.1109/AUPEC.2018.8757979.

[21] S. K. Rönnberg, A. G. Castro, A. Moreno-Munoz, M. H. J. Bollen, and J. Garrido, "Solar PV inverter supraharmonics reduction with random PWM," in *2017 11th IEEE International Conference on Compatibility, Power Electronics and Power Engineering (CPE-POWERENG)*, 4-6 April 2017 2017, pp. 644-649, doi: 10.1109/CPE.2017.7915248.

[22] M. M. AlyanNezhadi, H. Hassanpour, and F. Zare, "Grid-impedance estimation in high-frequency range with a single signal injection using time–frequency distribution," *IET Science, Measurement & Technology,* vol. 13, no. 7, pp. 1009-1018, 2019, doi: 10.1049/iet-smt.2018.5617.